High-precision nuclear magnetic resonance probe suitable for *in situ* studies of high-temperature metallic melts

Ao Li(李傲), Wei Xu(许巍), Xiao Chen(陈霄), Bing-Nan Yao(姚冰楠), Jun-Tao Huo(霍军涛), Jun-Qiang Wang(王军强), and Run-Wei Li(李润伟)

Citation: Chin. Phys. B, 2022, 31 (**4**): 040706. DOI: 10.1088/1674-1056/ac4a70
Journal homepage: http://cpb.iphy.ac.cn; http://iopscience.iop.org/cpb

What follows is a list of articles you may be interested in

Investigating the thermal conductivity of materials by analyzing the temperature distribution in diamond anvils cell under high pressure

Caihong Jia(贾彩红), Min Cao(曹敏), Tingting Ji(冀婷婷), Dawei Jiang(蒋大伟), and Chunxiao Gao(高春晓)
Chin. Phys. B, 2022, 31 (**4**): 040701. DOI: 10.1088/1674-1056/ac29aa

Cascaded dual-channel fiber SPR temperature sensor based on liquid and solid encapsulations

Yong Wei(魏勇), Lingling Li(李玲玲), Chunlan Liu(刘春兰), Jiangxi Hu(胡江西), Yudong Su(苏于东), Ping Wu(吴萍), and Xiaoling Zhao(赵晓玲)
Chin. Phys. B, 2021, 30 (**10**): 100701. DOI: 10.1088/1674-1056/ac0426

Microwave coherent manipulation of cold atoms in optically induced fictitious magnetic traps on an atom chip

Feng Zhou(周锋), Xiao Li(李潇), Min Ke(柯敏), Jin Wang(王谨), Ming-Sheng Zhan(詹明生)
Chin. Phys. B, 2017, 26 (**9**): 090701. DOI: 10.1088/1674-1056/26/9/090701

Spectroscopic measurements and terahertz imaging of the cornea using a rapid scanning terahertz time domain spectrometer

Wen-Quan Liu(刘文权), Yuan-Fu Lu(鲁远甫), Guo-Hua Jiao(焦国华), Xian-Feng Chen(陈险峰), Zhi-Sheng Zhou(周志盛), Rong-Bin She(佘荣斌), Jin-Ying Li(李金瑛), Si-Hai Chen(陈四海), Yu-Ming Dong (董玉明), Jian-Cheng Lü(吕建成)
Chin. Phys. B, 2016, 25 (**6**): 060702. DOI: 10.1088/1674-1056/25/6/060702

INSTRUMENTATION AND MEASUREMENT

High-precision nuclear magnetic resonance probe suitable for *in situ* studies of high-temperature metallic melts

Ao Li(李傲)[1,†], Wei Xu(许巍)[1,†‡], Xiao Chen(陈霄)[1,†], Bing-Nan Yao(姚冰楠)[1], Jun-Tao Huo(霍军涛)[1], Jun-Qiang Wang(王军强)[1,2,§], and Run-Wei Li(李润伟)[1,2]

[1] *CAS Key Laboratory of Magnetic Materials and Devices, and Zhejiang Province Key Laboratory of Magnetic Materials and Application Technology, Ningbo Institute of Materials Technology and Engineering, Chinese Academy of Sciences, Ningbo* 315201, *China*

[2] *Center of Materials Science and Optoelectronics Engineering, University of Chinese Academy of Sciences, Beijing* 100049, *China*

(Received 10 December 2021; revised manuscript received 9 January 2022; accepted manuscript online 12 January 2022)

High-temperature nuclear magnetic resonance (NMR) has proven to be very useful for detecting the temperature-induced structural evolution and dynamics in melts. However, the sensitivity and precision of high-temperature NMR probes are limited. Here we report a sensitive and stable high-temperature NMR probe based on laser-heating, suitable for *in situ* studies of metallic melts, which can work stably at the temperature of up to 2000 K. In our design, a well-designed optical path and the use of a water-cooled copper radio-frequency (RF) coil significantly optimize the signal-to-noise ratio (S/NR) at high temperatures. Additionally, a precise temperature controlling system with an error of less than ±1 K has been designed. After temperature calibration, the temperature measurement error is controlled within ±2 K. As a performance testing, ^{27}Al NMR spectra are measured in Zr-based metallic glass-forming liquid *in situ*. Results show that the S/NR reaches 45 within 90 s even when the sample's temperature is up to 1500 K and that the isothermal signal drift is better than 0.001 ppm per hour. This high-temperature NMR probe can be used to clarify some highly debated issues about metallic liquids, such as glass transition and liquid–liquid transition.

Keywords: high-temperature NMR probe, laser beams, temperature measurement, metallic melts

PACS: 07.57.Pt, 61.25.Mv, 76.60.−k **DOI:** 10.1088/1674-1056/ac4a70

1. Introduction

Investigations of dynamic relaxation over different timescales are crucial for understanding the natures of various materials such as glasses.[1–3] Nuclear magnetic resonance (NMR) is a unique tool that can characterize the structures and dynamics over a wide range of timescales in solids and liquids.[4–7] The extension of NMR to a high-temperature range provides a good opportunity to study the details of the structure and dynamics of various materials in liquid states such as silicates,[8,9] oxides,[10] molten salts,[11,12] and metallic liquids.[13–16] The success of high-temperature NMR experiments depends significantly on designing a suitable NMR probe, collecting the valid NMR spectra of the observed nuclei, and providing a stable high-temperature environment for the sample studied. However, for NMR, introducing high temperatures poses severe technical challenges. Specifically, besides the size limitation of bores of high-field superconducting magnets and the tricky high-temperature measurements, the compromise between the signal-to-noise ratio (S/NR) and the achievable sample temperature is an unavoidable problem, which has been previously reviewed in detail.[17–20] Nonetheless, over the past decades, many dedicated high-temperature NMR probes employing resistive heating,[17,18,21–23] laser or optical heating,[24–26] or other heating units,[27,28] have been designed, some of which can even reach 2200 K.[29,30]

Recently, *in situ* high-temperature NMR measurements of metallic melts and supercooled liquids have aroused great interest because it leads to an improved understanding of the role of temperature-induced structural evolution and dynamic crossover in glass transition,[15,16,31] liquid–liquid phase transition,[32,33] and melt heredity.[12,34] However, NMR observations of nuclei in metallic melts often pose more complex challenges than in non-metallic melts. The skin effect in metals significantly lowers the efficiency of the transverse oscillating magnetic field exciting the observed nuclei.[35] Furthermore, various complex interactions in metals, such as dipolar and indirect interactions between nuclei, also make it hard to observe the resonance from some nuclei or even all nuclei,[36,37] although in liquid states, these interactions are significantly motionally averaged out. Due to the above mentioned problems, *in situ* NMR measurements of metallic melts are usually very time-consuming because an accumulation of many scans is required to get a valid spectrum. Therefore, a complete and successful high-temperature NMR measurement requires a probe with good sensitivity and stability, even working at high temperature for a long time.

In the present work, we design a highly sensitive and pre-

[†]These authors contributed equally.

[‡]Corresponding author. E-mail: weixu@nimte.ac.cn

[§]Corresponding author. E-mail: jqwang@nimte.ac.cn

cise high-temperature ($T_{max} > 2000$ K) NMR probe, which remains stable in continuous operation at high temperatures and is thus suitable for *in situ* investigations of metallic melts. The probe employs two symmetrical and horizontal CO_2 laser beams as a heating element. A well-designed optical path not only ensures that the sample is uniformly heated but also enables the use of a more sensitive solenoidal RF coil. Meanwhile, using a fine thin-walled, water-cooled copper tube to wind RF coils significantly increases the S/NR under high-temperature conditions. Through computer programming and with the use of proportional-integral-derivative (PID) temperature controller, the rapid feedback adjustment between laser power (controlled by duty cycle) and the sample temperature is achieved, which reduces the temperature oscillation to $<$ $\pm$1 K. The temperature measurement error is controlled within $\pm$2 K after the temperature calibration by heating various pure metals to melting. The probe's performance is demonstrated by the ^{27}Al spectra acquired *in situ* from $Cu_{40}Zr_{40}Al_{20}$ equilibrium melts at different temperatures. Even above 1500 K, the S/NR of the ^{27}Al NMR spectra could reach 45 with only 512 scans (about 90 s).

2. Description of probe

As shown in Fig. 1(a), our High-temperature NMR apparatus mainly consists of the homemade laser-heating probe, a cryogen free superconducting 9.4 T magnet for NMR with the homogeneity sufficiently to achieve few ppm (below 10 ppm in the radial profile in a region of 20 mm diameter sphere), and a NMR console which controls the NMR spectrometer to aquire the spectra. In our design, the heating element of the high-temperature NMR probe consists of two computer-controlled 50 W CO_2 laser sources. Compared to the conventional resistance heating method, the use of laser beams has obvious advantages, which have been reviewed in detail previously.[20] As shown in Fig. 1(a), two laser beams are fed horizontally and symmetrically from the top of the magnet. They are first reflected by 45° reflectors, then focused by ZnSe lenses, and finally shot vertically into the probe residing in the bore of the superconducting magnet. A laser pointer (red light), collinear with the primary laser, provides a visualization of the optical path, enabling the adjustment of the laser beams to their target positions. Inside the probe, as sketched in Fig. 1(b), two vertical laser beams pass through the transparent ZnSe windows, and then are reflected by 45° copper mirrors on the water-cooled base plate, and finally symmetrically irradiate horizontally on both sides of the sample holder. Symmetrical irradiation ensures a better thermal homogeneity of the samples. More importantly, such a design of the optical path allows the use of a solenoidal RF coil.[38,39] with higher sensitivity, a stronger RF field, and a better homogeneity instead of a saddle-shaped RF coil used in previous laser-heating probes.[30,40]

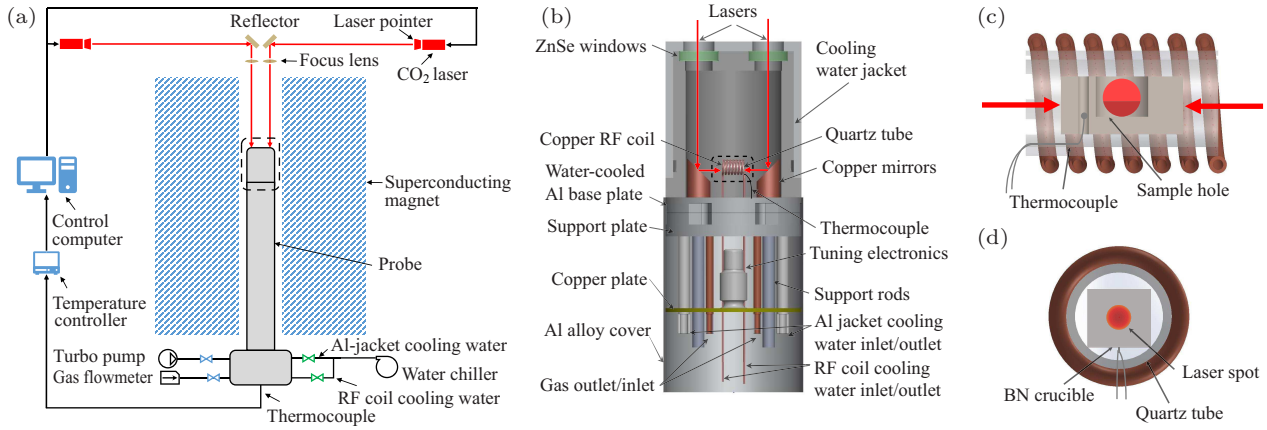

Fig. 1. Schematic diagram of high-temperature NMR experimental setup based on laser-heating. (a) Simplified drawing of high-temperature NMR apparatus including laser-heating system, temperature monitoring and controlling system, high-temperature probe and 9.4 T superconducting magnet. (b) Cross-section of the high-temperature probe-head (black dashed frame in (a)). (c), (d) Schematic construction diagram of the RF coil (the black dotted frame in (b)).

Herein, the RF coil of our high-temperature probe is a 7-turn solenoid with an inner diameter of 6 mm, as shown in Figs. 1(c) and 1(d). The RF coil is made by winding a fine water-cooled, thin-walled copper tube with a diameter of 1 mm. It is connected to a water chiller so that the RF coil can remain cold despite working at a high sample temperature. According to the simplified formula for the signal-to-noise ratio ψ of an NMR experiment proposed by J. F. Stebbins,[17]

$$\psi = cV_s T^{-1/2} \rho^{-1/4} V_c^{-\alpha}, \tag{1}$$

the S/NR is strongly dependent on the temperature T, the resistivity ρ at T, and the fill factor (the ratio of sample volume V_s to coil volume V_c) of the RF coil. Hence, the application of the water-cooled RF coil poses apparent advantages. First, the thermal noise from a heated RF coil can be significantly suppressed, which guarantees a high signal quality at

high temperatures. Second, the RF coil can be made of metals with better conductivity, such as copper or silver, rather than the refractory but very low conductive metals used in previous designs.[22,41] Third, no other thermal insulation, except the quart tube, is required between the coil and the sample holder, maximizing the filling factor. Lastly, as other RF electronic components are placed on a copper plate outside the double-walled water-cooled chamber made of aluminum alloy, such a design minimizes the impact of the waste heat from the sample holder.

As shown by Fig. 1(c), the sample holder is placed horizontally inside the RF coil, and a quartz tube is put between them. High-purity hexagonal boron nitride is selected as the material of the sample holder because it is an excellent dielectric, highly thermally conductive, and nonreactive with metals, which has been used in laser-heating experiments since a long time ago.[24,25] Thanks to the high energy efficiency of laser irradiation and the high thermal conductivity of the boron nitride, the sample holder acts as a small but powerful furnace, which can quickly heat the samples in it. The boron nitride crucible is machined into a cuboid with a size of 7 mm × 3.5 mm × 3.5 mm. As presented in Fig. 1(d), only two edges of the sample holder are in contact with the quartz tube, which minimizes the heat conduction between the crucible and the coil. As shown in Fig. 1(c), the thermocouple is inserted in the hole drilled into the boron nitride crucible and located close to the sample. This configuration ensures that the measured temperature is close to the actual temperature of the sample. Nonetheless, temperature calibration is necessary for high precision, which will be discussed in detail later. The thermocouple used here is the Wu–Re thermocouple, specially made for high-temperature measurements.

In addition, preventing samples' oxidation at high temperatures is crucial for obtaining valid data in NMR *in situ* studies of metallic melts. In each high-temperature NMR experiment, the chamber is flushed with 99.999% high-purity argon gas more than five times after the sample is loaded. Then the chamber is pumped to a high vacuum better than 10^{-5} Pa by a turbopump. Next, high-purity inert or reducing gas is injected into the chamber to a pressure of about 0.1 Pa, which is helpful to minimize the volatilization of the molten metals. When the crucible is heated, the gas temperature inside the probe is expected to remain below 500 °C owing to the cooling of the cooling-water jacket. Assuming that the pressure is proportional to the temperature, the pressure is expected to increase by 2–3 times, namely, 0.2–0.3 Pa, which is still lower than the ambient pressure. The experimental results to be shown in Subsection 4.2 will also clarify that ^{27}Al NMR spectra have perfect Lorentzian line shapes, which indicates that the gas tightness of our probe is good enough, even for Zr-based alloys that are easily oxidized.

3. Temperature control and calibration

3.1. Temperature control

Precise control and determination of the sample temperature are essential for the successful capture of the potential structural change or dynamics crossover in melts and the subsequent interpretation of the experimental data. As shown in Fig. 2(a), through computer programming and using the PID temperature controller, we have established a rapid feedback adjustment system between the laser power (duty cycle) and the temperature measured by the thermocouple. This system is used to control the sample temperature accurately. As shown by Fig. 2(b), the temperature fluctuation can still be controlled within ±1 °C even at 1500 °C, which is crucial for isothermal measurements of equilibrium melts.

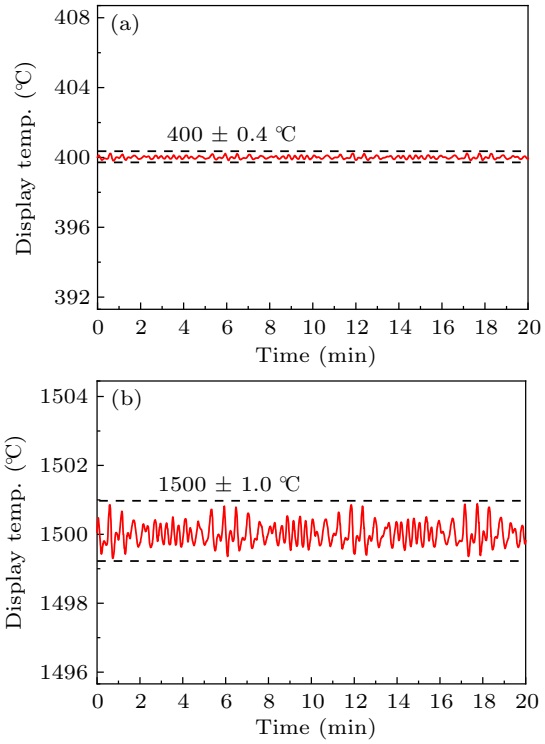

Fig. 2. Temperature profile during isothermal tests at (a) 400 °C and (b) 1500 °C, respectively. The dashed lines represent the upper and lower limits of the temperature fluctuation.

3.2. Temperature monitoring and calibration

A common approach to accurately determine the temperature is via NMR-observable phase transitions, which is suitable for the NMR experiments below 900 °C.[42–44] Optical pyrometers, usually used in laser-heating experiments,[30] are not employed in our design because they have lower accuracy than thermocouples, and their use is unpractical for our probe since the sample is located in an opaque chamber. In our scenario, the thermocouple is used to monitor the sample temperature. Here we calibrate the sample temperature through the perturbations on the temperature ramping rate curves caused by the latent heat of fusion of a range of pure metals. Figure 3 shows the heating curve of pure Cu during high-temperature

NMR experiments. When the solid copper melts, there is an instantaneous over-compensation of laser power in response to the latent heat, resulting in a spike (as indicated by the orange arrow) on the temperature ramping rate curve (blue line), while the change in the temperature ramping curve induced by this over-compensation (as displayed in the right inset) is weak. The evolution of ^{63}Cu NMR spectra also proves the occurrence of melting. As shown by the right inset, the peak position (Knight shift) of ^{63}Cu NMR spectra changes abruptly from 2500 ppm to 2615 ppm, accompanied by an evident narrowing of peak linewidth after melting, which has been previously reported in detail.[45,46]

Hence, it is reasonable to assume that the onset temperature of the spike on the temperature ramping rate curve corresponds to the melting point of the pure metals. Therefore, we carried out the same heating operation for pure In, Zn, Al, Ag, Pd as shown in Figs. 4(a)–4(e), respectively. Subsequently, a temperature calibration curve is obtained over a wide range of 100 °C to 1600 °C, as displayed in Fig. 4(f). The data were well fitted using a linear relationship

$$T = 9.512 + 1.069 \times T_{\mathrm{D}}, \tag{2}$$

where T is the sample temperature (°C), and T_{D} is the display temperature.

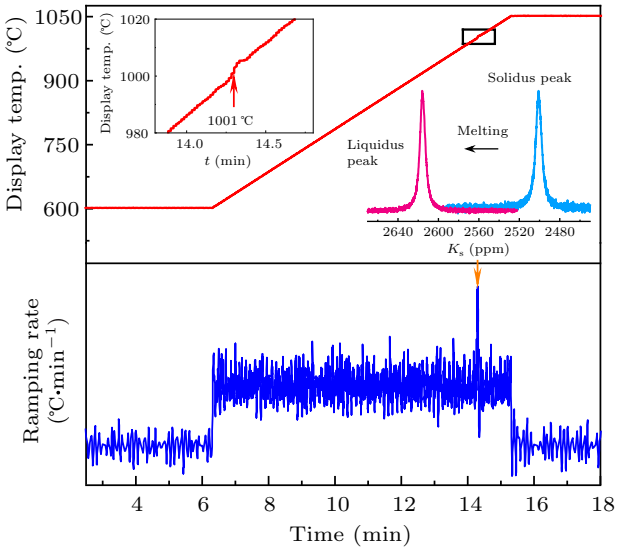

Fig. 3. Temperature profile (upper panel) at 50 K/min and the corresponding ramping rate curve (lower panel) for the high-temperature NMR experiments of pure copper. The ramping rate is taken from the differential of the temperature curve. The right inset is the magnified image of the black line frame on the temperature curve. The left inset displays the ^{63}Cu NMR spectra before and after melting.

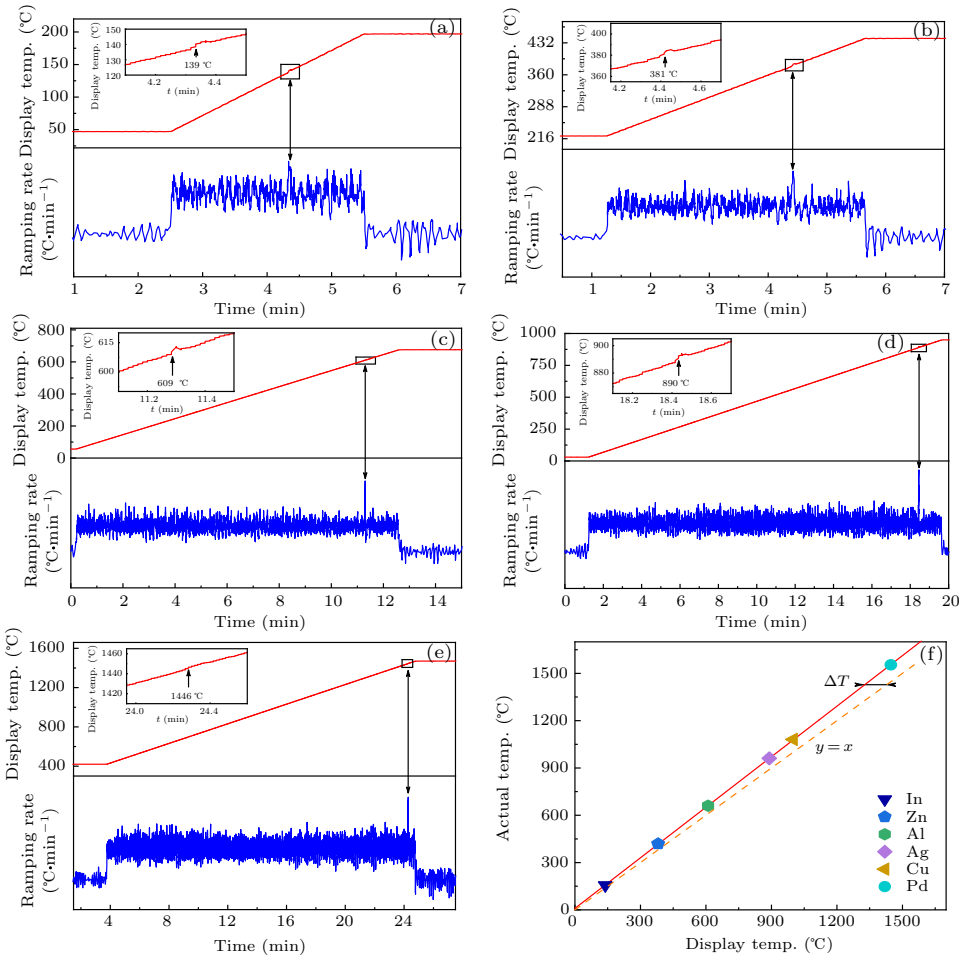

Fig. 4. (a)–(e) The temperature profiles (red line) and the corresponding ramping rates (blue line) for heating In, Zn, Al, Ag, Pd, respectively. The insets are the magnified images of the black line frames on the temperature curve. The black arrow indicates the display temperatures when pure metals melt. (f) The theoretical melting points of In, Zn, Al, Ag, Cu, Pd are plotted against their corresponding display temperatures. The red line represents the fitting calibration curve. The dashed orange line ($y = x$) demonstrates the change of ΔT with increasing temperature.

High-temperature NMR experiments of pure aluminum and copper are carried out to verify the temperature accuracy after calibration because their melting points can be easily determined by the abrupt change of Knight shift (K_s) in NMR spectra. As shown in Fig. 5(a), when the Al melts, the co-existence of the Al liquidus peak (1606 ppm, reference: 1 mol^{-1} $AlCl_3$ aqueous solution) and the Al solidus peak (1641 ppm) can be observed in ^{27}Al NMR spectra. As the melting process progresses, the intensity of the liquidus peak increases, while the intensity of the solidus peak decays and finally disappears. Similarly, we can observe the jump of the K_s from 2500 ppm to 2615 ppm (reference: 1 mol^{-1} CuBr aqueous solution) and the co-existence of two phases in the ^{63}Cu NMR spectra as shown in Fig. 5(b). However, unlike the negative shift of K_s in ^{27}Al NMR spectra, the K_s of ^{63}Cu suddenly increases when solid copper melts.[46,47] By comparing the melting points measured by our calibrated NMR probe to the literature values, the temperature measurement error is determined to be less than ± 2 K. Moreover, during such a short time of sample melting, the co-existence of solidus and liquidus phases can be captured, which fully proves the excellent sensitivity of the probe.

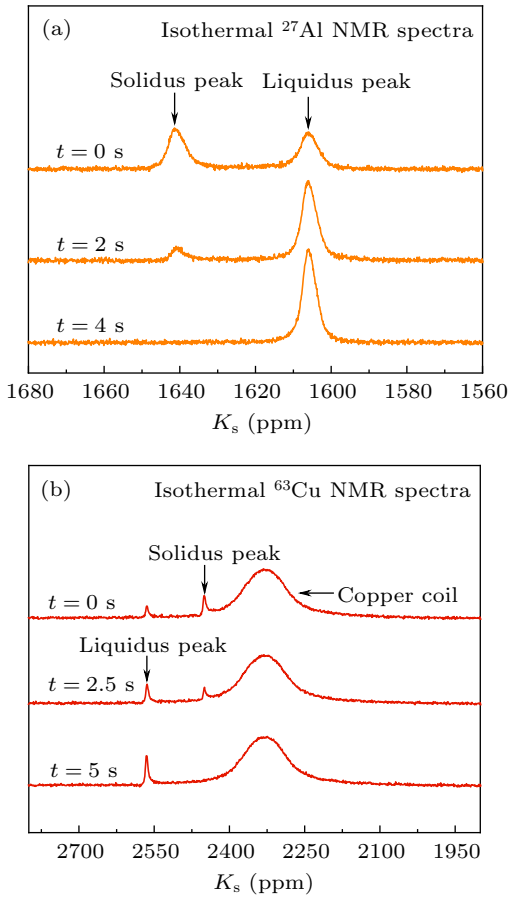

Fig. 5. NMR spectra of pure Al and Cu during melting. (a) ^{27}Al NMR spectra of pure Al during melting. (b) ^{63}Cu NMR spectra of pure Cu during melting. The broad peak at 2376 ppm is the peak of the copper coil.

4. Experimental results and device performance

To quantitatively characterize the performance of the high-temperature NMR probe, the ^{27}Al NMR spectra of $Cu_{40}Zr_{40}Al_{20}$ melt were measured *in situ*. Cu–Zr-based alloy is a typical metallic glass-forming system that has been intensively studied from the perspective of dynamics and structure of the melt.[48–53]

4.1. Materials and high-temperature NMR experiments

The $Cu_{40}Zr_{40}Al_{20}$ metallic rods with a diameter of 2 mm were prepared under argon atmosphere by water-cooled copper mold casting using high-purity ingredients of Cu, Zr, and Al (purity $>$ 99.99 wt%). The liquidus temperature of $Cu_{40}Zr_{40}Al_{20}$ is determined to be 1185 K by differential scanning calorimeter (DSC). A single sample was cut from the as-cast sample for the following high-temperature NMR experiments. The cut sample was overheated to 1530 K (about 345 K above the liquidus temperature), and then ^{27}Al spectra were acquired at an interval of 40 K during the cooling and subsequent reheating process. A standard 90-degree single pulse sequence was used with pulse widths of 10 μs for ^{27}Al. Recycle delay time was 6 ms for all measurements. The same number of scans (512 scans about 90 s) were accumulated at each isothermal temperature to facilitate the following comparison of the signal-to-noise ratio. After the high-temperature NMR experiments, the sample preserved a shiny metallic surface, indicating that the sample was not severely oxidized.

4.2. Results and discussion

As shown in Figs. 6(a) and 6(b), all ^{27}Al NMR spectra above the liquidus temperature show single narrow peaks of Lorentzian shape, which means that the melt is homogeneous and is heated uniformly. The NMR peak intensity (the integrated area of the peak) does not reduce much as the temperature rises. The temperature dependence of S/NR is obtained and presented in Fig. 6(c). The S/NR remains above 45, even at a high temperature of 1530 K, which is good enough to obtain valid information from NMR spectra. Such a high precision at high temperatures is attributed to the efficient cooling system of the RF coil. To highlight the improvement of our design, here we compare the sensitivity of our probe and that of the traditional resistance heating probe without water-cooling under the same number of scans. As shown in the inset of Fig. 6(c), the ^{27}Al spectrum obtained by our probe shows a S/NR of about 120% higher than that of the resistance-heating probe, and also has a better Lorentzian line shape. In addition, to characterize the stability of the probe, the $Cu_{40}Zr_{20}Al_{20}$ melt was held at 1530 K for about 6 hours, and ^{27}Al NMR spectra were acquired at intervals of 3 min. The isothermal K_s

fluctuation against the time is plotted in Fig. 6(d). The fluctuation amplitude is within ± 0.1 ppm, which demonstrates the excellent stability of the probe. The signal drift is fitted as about -0.0007 ppm per hour, which is consistent with the magnetic field drift of the superconducting magnet[54] and can guarantee long-time tests.

The valuable information extracted from NMR spectra mainly includes the temperature dependences of K_s and linewidth $\Delta\nu_{1/2}$ (full width at half maximum of the Lorentzian-shaped spectra), which represent two dynamics at different timescales, respectively. To the best of our knowledge, K_s is sensitive to the vibrational and atomic cage-rattling motion, which has been proved to be associated with the fast β process in glass-forming metallic liquids under mode-coupling theory (MCT) frame.[15] In addition, the information about the electronic structure of observed nuclei could be obtained by combining K_s with the magnetic relaxation rate by Korringa relation.[15,33,34] For quadrupolar nuclei such as ^{27}Al with spin quantum number $I = 5/2$, the coupling between the electric-field gradient (EFG) and electric quadrupole moment of nuclei gives rise to efficient spin-lattice relaxation. Since the diffusion of all atoms neighboring observed nuclei could cause fluctuations of EFG tensor at the observed nuclei sites, the quadrupolar spin-lattice relaxation (R_Q) is proved to be very effective in probing atomic diffusion in liquid metals.[55,56] Unlike K_s, the correlation function of EFG captures the essence of cage collapsing in glass-forming metallic liquids which is at longer timescales than the β process.[16] In the fast motion limit, R_Q can be derived from the measured spectral linewidth, described clearly in the literature.[33,55] Herein, we obtain the K_s and $1/R_Q$ of ^{27}Al at different temperatures, as shown in Fig. 7.

The temperature dependences of K_s and $1/R_Q$ are reversible during cooling and reheating, implying that the melt is stable during NMR experiments. Meanwhile, the results strongly support that the temperature control and monitoring system is as accurate as described above. K_s and $1/R_Q$, taken from ^{27}Al NMR spectra, vary linearly with temperature, demonstrating that no structural or dynamic crossover occurs in the melt in the measured temperature range as reported previously.[49,57]

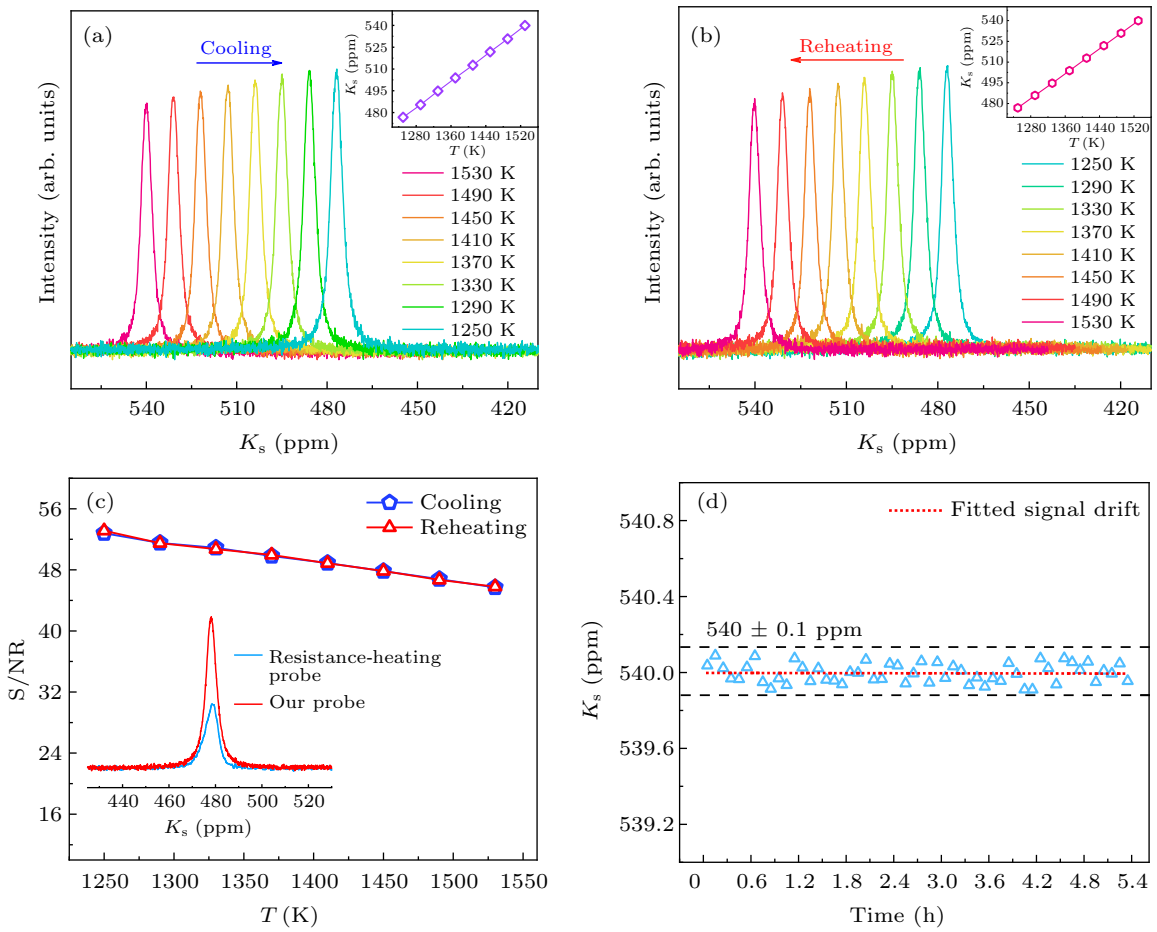

Fig. 6. ^{27}Al NMR spectra of $Cu_{40}Zr_{40}Al_{20}$ at various temperatures above the liquidus temperature. Spectra are of perfect Lorentzian line shape. (a) ^{27}Al NMR spectra during cooling from 1530 K. (b) ^{27}Al NMR spectra during reheating from 1250 K. (c) S/NR of ^{27}Al spectra at various temperatures during cooling and reheating process. Errors are less than the size of the symbols where error bars are not shown explicitly. The inset shows the comparison between the present NMR spectrum and the spectrum obtained by the traditional resistanceheating probe. (d) K_s fluctuation during isothermal measurements at 1530 K. The dashed lines represent the upper and lower limits of K_s fluctuation. The slope of the red dotted line represents the signal drift.

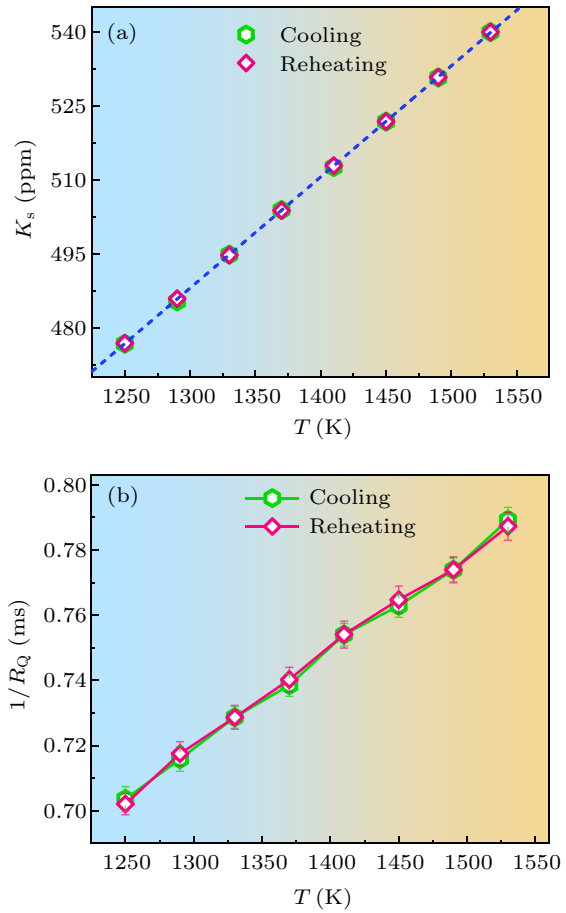

Fig. 7. Temperature dependences of ^{27}Al K_s and $1/R_Q$ during cooling and reheating in the temperature range of 1250–1550 K. (a) Temperature dependence of ^{27}Al K_s during cooling and reheating. The blue dashed line represents the fitting curve of K_s versus T with a slope of 0.22 ppm/K. (b) Temperature dependence of $1/R_Q$ during cooling and reheating.

5. Conclusions

In summary, a highly sensitive, precise, and stable high-temperature NMR probe that employs two CO_2 laser beams as the heating elements has been designed. With this high-temperature NMR apparatus, we carry out *in situ* isothermal NMR measurements on $Cu_{40}Zr_{40}Al_{20}$ melt and obtain the S/NR, the temperature dependence of the K_s, and line width of ^{27}Al NMR spectra. The probe is demonstrated to be capable of maintaining S/NR above 45 even above 1500 K. It shows that the use of a water-cooled RF coil with a solenoidal geometry significantly improves S/NR at high temperatures compared with the previously reported high-temperature NMR probes. The reversible ^{27}Al NMR spectra during cooling and reheating also verify the probe's accurate temperature controlling and monitoring. Moreover, the atmosphere and pressure in the closed chamber of the probe can be adjustable depending on the problems to be solved. Future applications of our high-temperature NMR probe can be extended to studies of molten salts, hydrogen storage material, or high-temperature fuel cells, not limited to metallic systems.

Acknowledgments

Project supported by the Instrument Developing Project of the Chinese Academy of Sciences (Grant No. YZ201639), the National Key R&D Program of China (Grant No. 2018YFA0703604), the National Natural Science Foundation of China (Grant Nos. 51922102, 92163108, and 52071327), and the Zhejiang Provincial Natural Science Foundation of China (Grant No. LR18E010002).

References

[1] Wang W H 2019 *Prog. Mater. Sci.* **106** 100561
[2] Cao Y, Song L, Li A, Huo J, Li F, Xu W and Wang J Q 2020 *Sci. Chin. Phys. Mech. & Astron.* **63** 276113
[3] Cao L, Song L J, Cao Y R, Xu W, Huo J T, Lu Y Z and Wang J Q 2021 *Chin. Phys. B* **30** 076103
[4] Mu C, Yin Q, Tu Z, Gong C, Lei H, Li Z and Luo J 2021 *Chin. Phys. Lett.* **38** 077402
[5] Shao Y T, Hong W S, Li S L, Li Z and Luo J L 2019 *Chin. Phys. Lett.* **36** 127401
[6] Fan G Z, Chen R Y, Wang N L and Luo J L 2015 *Chin. Phys. Lett.* **32** 077203
[7] Luo J, Yang J, Maeda S, Li Z and Zheng G Q 2018 *Chin. Phys. B* **27** 077401
[8] Stebbins J F and Farnan I 1992 *Science* **255** 586
[9] George A M and Stebbins J F 1998 *Am. Mineral.* **83** 1022
[10] Massiot D, Fayon F, Montouillout V, Pellerin N, Hiet J, Roiland C, Florian P, Coutures J P, Cormier L and Neuville D R 2008 *J. Non. Cryst. Solids* **354** 249
[11] Shakhovoy R, Sarou-Kanian V, Rakhmatullin A, Véron E and Bessada C 2015 *J. Appl. Phys.* **118** 243906
[12] Liu X, Liu S, Chen E, Peng L and Yu Y 2019 *J. Phys. Chem. Lett.* **10** 4285
[13] Warren-Jr W W and Wernick J H 1971 *Phys. Rev. B* **4** 1401
[14] El-Hanany U and Zamir D 1972 *Phys. Rev. B* **5** 30
[15] Li L, Schroers J and Wu Y 2003 *Phys. Rev. Lett.* **91** 265502
[16] Li L and Wu Y 2008 *J. Chem. Phys.* **128** 052307
[17] Stebbins J F, Schneider E, Murdoch J B, Pines A and Carmichael I S E 1986 *Rev. Sci. Instrum.* **57** 39
[18] Adler S B, Michaels J N and Reimer J A 1990 *Rev. Sci. Instrum.* **61** 3368
[19] Stebbins J F 1991 *Chem. Rev.* **91** 1353
[20] Kirchhain H and van Wüllen L 2019 *Prog. Nucl. Magn. Reson. Spectrosc.* **114–115** 71
[21] Hafner S and Nachtrieb N H 1964 *Rev. Sci. Instrum.* **35** 680
[22] DeFries T H and Jonas J 1979 *J. Magn. Reson.* **35** 111
[23] Privalov A F and Lips O 2002 *Appl. Magn. Reson.* **22** 597
[24] Massiot D, Bessada C, Echegut P, Coutures J P and Taullele F 1990 *Solid State Ion.* **37** 223
[25] Rollet A L, Sarou-Kanian V and Bessada C 2009 *Inorg. Chem.* **48** 10972
[26] Ernst H, Freude D, Mildner T and Wolf I 1996 *Solid State Nucl. Magn. Reson.* **6** 147
[27] Maresch G G, Kendrick R D and Yannoni C S 1990 *Rev. Sci. Instrum.* **61** 77
[28] Poplett I J F, Smith M E and Strange J H 2000 *Meas. Sci. Technol.* **11** 1703
[29] Capron M, Florian P, Fayon F, Trumeau D, Hennet L, Gaihlanou M, Thiaudière D, Landron C, Douy A and Massiot D 2001 *J. Non. Cryst. Solids* **293–295** 496
[30] Massiot D, Trumeau D, Touzo B, Farnan I, Rifflet J C, Douy A and Coutures J P 1995 *J. Phys. Chem.* **99** 16455
[31] Tang X P, Geyer U, Busch R, Johnson W L and Wu Y 1999 *Nature* **402** 160
[32] Xu W, Sandor M T, Yu Y, Ke H B, Zhang H P, Li M Z, Wang W H, Liu L and Wu Y 2015 *Nat. Commun.* **6** 7696
[33] Peng L, Chen E, Liu S, Liu X and Yu Y 2019 *Phys. Rev. B* **100** 104113
[34] Chen E Y, Peng S X, Peng L, Di Michiel M, Vaughan G B, Yu Y, Yu H B, Ruta B, Wei S and Liu L 2021 *Scr. Mater.* **193** 117

[35] Iwashita Y and Icr K 2004 *Proceedings of the LINAC*, August 16–20,2004, Lübeck, Germany, p. 700
[36] Titman J M 1977 *Phys. Rep.* **33** 1
[37] Seymour E F W 1974 *Pure Appl. Chem.* **40** 41
[38] Hoult D I and Richards R 1976 *J. Magn. Reson.* **24** 71
[39] Arakawa M, Crooks L, Mc-Carten B, Hoenninger J, Watts J and Kaufman L 1985 *Radiology* **154** 227
[40] Moussaed G, Gobet M, Rollet A L, Sarou-Kanian V, Salanne M, Simon C and Bessada C 2010 *ECS Trans.* **33** 159
[41] Baker D B and Conradi M S 2005 *Rev. Sci. Instrum.* **76** 073906
[42] Wu J, Kim N and Stebbins J F 2011 *Solid State Nucl. Magn. Reson.* **40** 45
[43] Thurber K R and Tycko R 2009 *J. Magn. Reson.* **196** 84
[44] Jardón-Álvarez D and auf der Günne J S 2018 *Solid State Nucl. Magn. Reson.* **94** 26
[45] Warren-Jr W W and Clark W G 1970 *Phys. Rev. B* **1** 24
[46] El-Hanany U and Zamir D 1969 *Phys. Rev.* **183** 809
[47] El-Hanany U and Zamir D 1972 *Solid State Commun.* **10** 1223
[48] Zhao X, Wang C, Zheng H, Tian Z and Hu L 2017 *Phys. Chem. Chem. Phys.* **19** 15962
[49] Zhou C, Hu L, Sun Q, Qin J, Bian X and Yue Y 2013 *Appl. Phys. Lett.* **103** 171904
[50] Soklaski R, Tran V, Nussinov Z, Kelton K and Yang L 2016 *Philos. Mag.* **96** 1212
[51] Jaiswal A, O'Keeffe S, Mills R, Podlesynak A, Ehlers G, Dmowski W, Lokshin K, Stevick J, Egami T and Zhang Y 2016 *J. Phys. Chem. B* **120** 1142
[52] Bi Q L and Lv Y J 2014 *Chin. Phys. Lett.* **31** 106401
[53] Wen D, Deng Y, Gao M and Tian Z 2021 *Chin. Phys. B* **30** 076101
[54] Kryukov E, Bugoslavsky Y, Linde A J P, Holubar T, Burgess S, Marlow D and Good J 2020 *Solid State Nucl. Magn. Reson.* **109** 101684
[55] Warren-Jr W W and Clark W G 1969 *Phys. Rev.* **177** 600
[56] Kerlin A L and Clark W G 1975 *Phys. Rev. B* **12** 3533
[57] Chu W, Shang J, Yin K, Ren N, Hu L, Zhao Y and Dong B 2020 *Acta Mater.* **196** 690